

Supporting Information for

***Visual Detection of a Nerve Agent Simulant using Chemically  
Modified Paper Strips and Dye-Assembled Inorganic Nanocomposite***

*Nilanjan Dey<sup>a</sup>, Dr. Satadru Jha<sup>a</sup>, Santanu Bhattacharya<sup>\*,a,b</sup>*

<sup>a</sup>Department of Organic Chemistry, Indian Institute of Science, Bangalore 560 012, India

<sup>b</sup>Indian Association of Cultivation of Science, Kolkata 700032, India

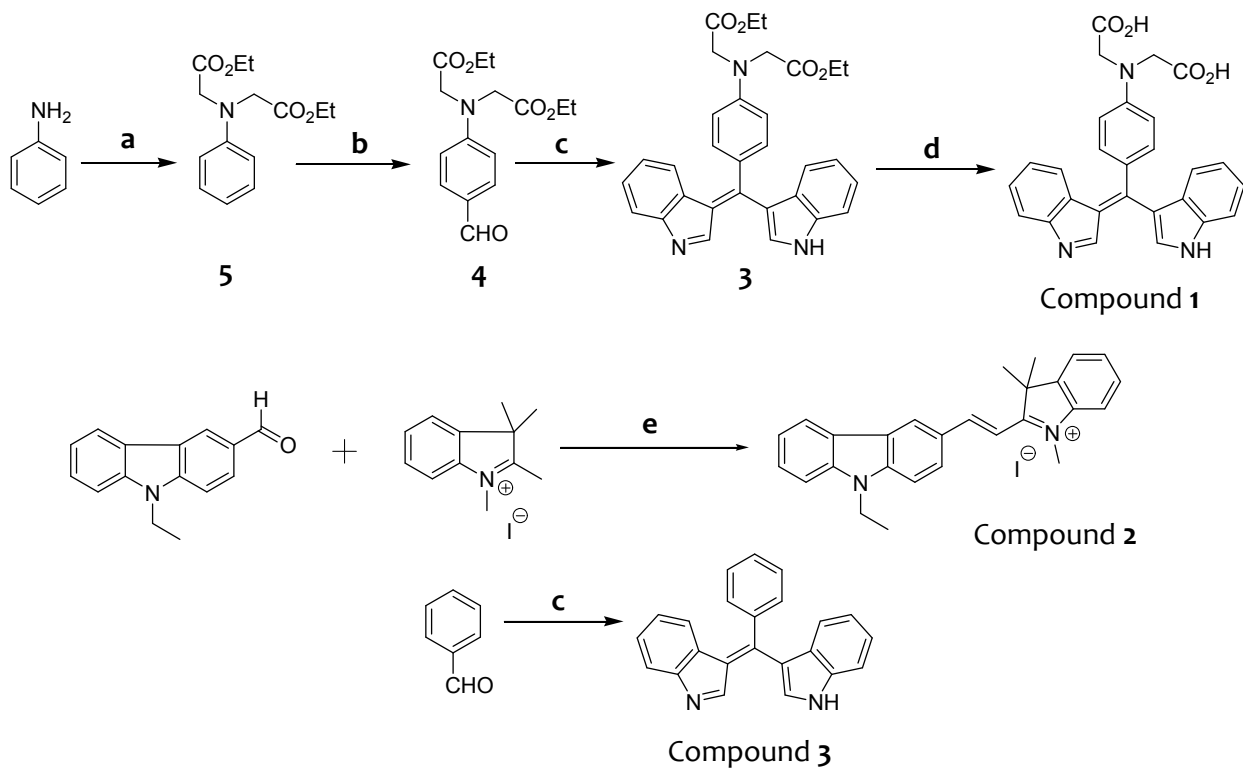
\*Corresponding Author Email: [sb@orgchem.iisc.ernet.in](mailto:sb@orgchem.iisc.ernet.in)

**Table of content**

Entry	Titles	Page Numbers
1	Synthesis of probe compounds	2
2	Comparison with other reported sensory systems	3
3	Additional spectral data	4-21

## Synthesis of probe compounds involved in present study

The synthesis of compound **1**<sup>[1]</sup> (along with precursors **5**, **4**, **3**)<sup>[2]</sup>, and **2**<sup>[3]</sup> were performed following the literature reported procedure.



**Scheme S1.** (a) Ethyl 2-bromoacetate, K<sub>2</sub>HPO<sub>4</sub>, CH<sub>3</sub>CN, reflux, 24 h; (b) POCl<sub>3</sub>/DMF, 90°C, 2 h; (c) I<sub>2</sub>/CH<sub>3</sub>CN, rt, 1 h and then DDQ/CH<sub>3</sub>CN, rt., 1 h; (d) Aqueous NaOH, reflux, 2h, then acidified with dil. HCl; (e) Piperidine, EtOH, reflux, 12 h.

#### References:

1. Kumari, N.; Jha, S.; Bhattacharya, S. A Chemodosimetric Probe Based on a Conjugated Oxidized Bis-Indolyl System for Selective Naked-Eye Sensing of Cyanide Ions in Water. *Chem. Asian J.* **2012**, *7*, 2805-2812.
2. Wang, S.; Fei, X.; Guo, J.; Yang, Q.; Li, Y.; Song, Y. A novel reaction-based colorimetric and ratiometric fluorescent sensor for cyanide anion with a large emission shift and high selectivity *Talanta* **2016**, *148*, 229-236.
3. He, X.; Hu, S.; Liu, K.; Guo, Y.; Xu, J.; Shao, S. Oxidized Bis(indolyl)methane: A Simple and Efficient Chromogenic-Sensing Molecule Based on the Proton Transfer Signaling Mode. *Org. Lett.*, 2006, *8*, 333–336.

#### Comparison of present method with other reported sensory systems for DCNP

The optical probes reported for selective sensing of diethyl cyanophosphonate (DCNP) is very few in number. Owing to the high hydration energy of the cyanide ion ( $\Delta H_{\text{hyd}} = -67$  kJ/ mol), these sensors could perform only in the organic or semi-aqueous environment. This essentially limits the applications of these probes in real-life biological systems. Thus, it is important to explore a "water-compatible" chemical reaction of cyanide ion in order to devise a new sensory system. The following table describes a comparison of the present method with the other reported sensory systems.

Entry	Mechanism of interaction	Response	Time	Medium	Reference
1	Nucleophilic addition of cyanide ion to carbonyl group	Pink to orange	Instantaneous	acetonitrile	Org. Biomol. Chem., 2014, 12, 8745–8751
2	CN <sup>-</sup> triggered deprotonation of NH group	Colorless to yellow	10 min	THF	Analyst, 2011, 136, 5151–5156
3	Cyanide catalyzed migration of the phosphate group from the pyridine to the aniline nitrogen	Pale orange to yellow	2 min	Acetonitrile/ water (25:75 v/v)	Chem. Eur. J. 2011, 17, 6931 – 6934
4	Tandem phosphorylation followed by cyanohydrin reaction	Yellow to blue green	1 h	DMSO	RSC Adv., 2014, 4, 24645–24648
5	Relay recognition ability for DCNP via the formation of a six-member cyclic Product formation	Green to cyan emission	1 min	CH <sub>3</sub> CN/H <sub>2</sub> O (5/5, v/v)	RSC Adv., 2016, 6, 18711–18717
6	Cyanide induced Michael addition reaction to the electron deficient C=C bond	Red to color less	~20 min	water	Present work

**Table S1.** A comparison of the present method with the reported sensory systems (specific for DCNP).

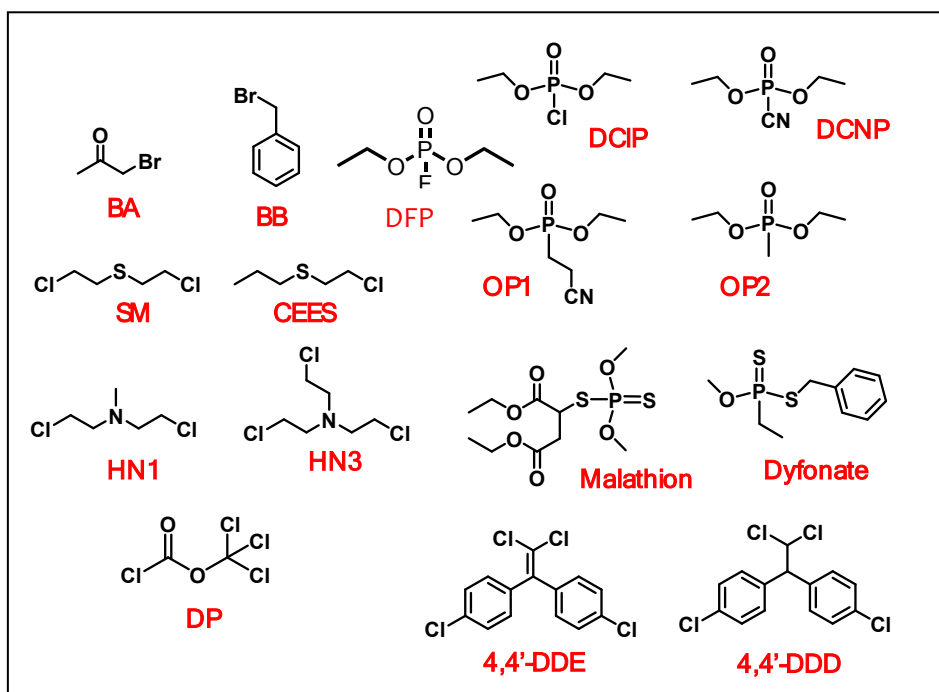


**Figure S1.** Structure of different analytes involved in present study.

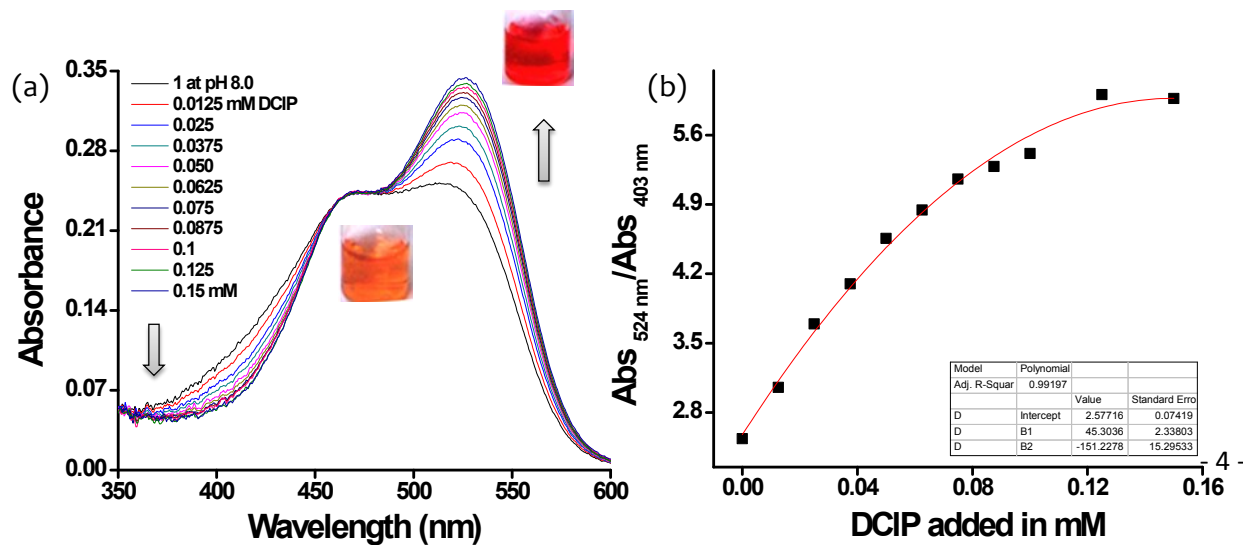


**Figure S2.** (a) UV-visible titration of **1** (20  $\mu\text{M}$ ) with DCIP (0 - 0.15 mM) at pH 8.0 in water. (b) Ratiometric response of **1** (20  $\mu\text{M}$ ) during titration of DCIP (0 - 0.15 mM) at pH 8.0 in water.

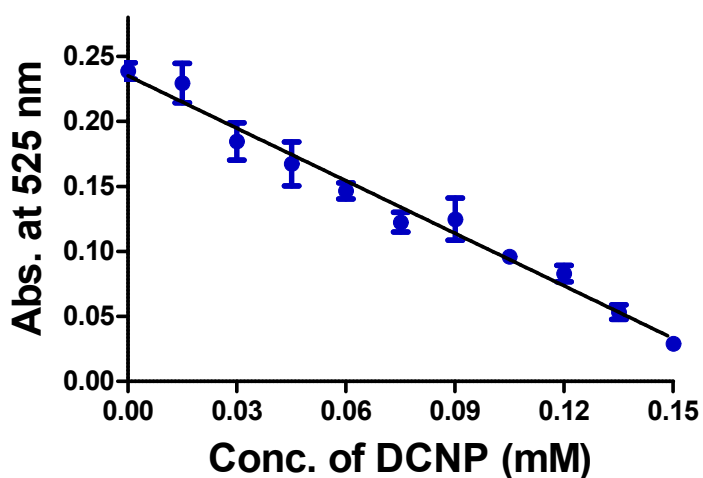


**Figure S3.** Change in absorbance of **1** (20  $\mu\text{M}$ ) at 525 nm upon addition of DCNP (0 - 0.15 mM) at pH 8.0 in water. (Each value was recorded after 30 min incubation).

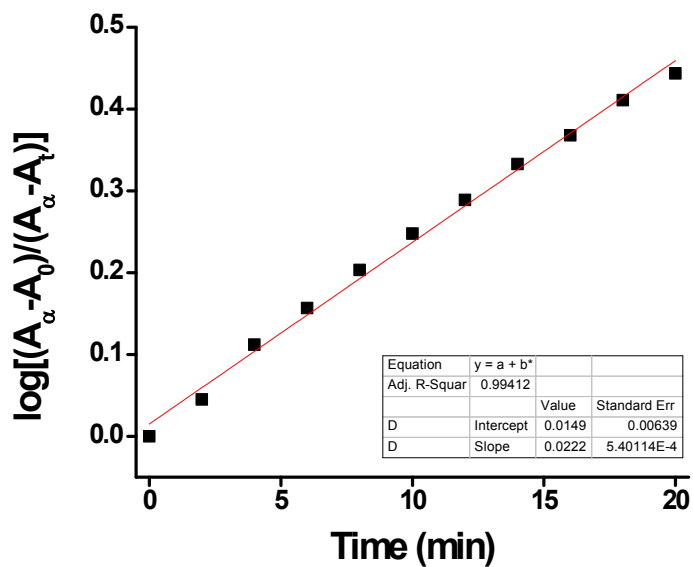


**Figure S4.** Determination of 1<sup>st</sup> order rate constant during interaction of **1** with DCNP at pH 8.0 in water (at 25 °C). Rate constant:  $(5.06 \pm 0.05) \times 10^{-2} \text{ min}^{-1}$ .

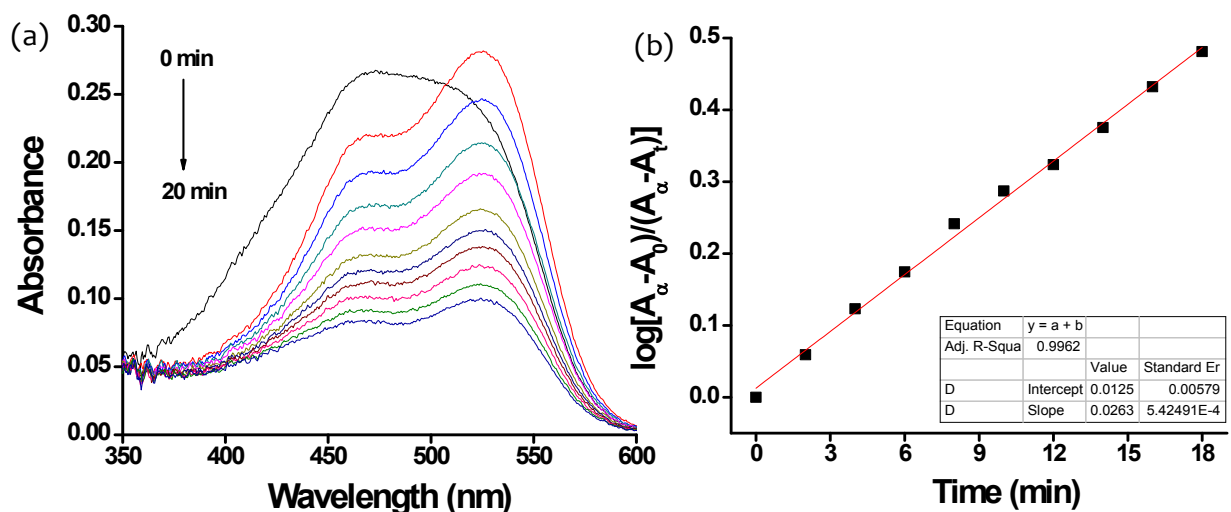


**Figure S5.** (a) Changes in UV-visible spectra of **1** (20  $\mu\text{M}$ ) with time upon addition of 0.25 mM of DCNP in water (pH 8.0) at 35 °C. (b) Plot of  $\text{Abs}_{525 \text{ nm}}$  against time shows 1st Order reaction. Rate constant:  $(6.06 \pm 0.05) \times 10^{-2} \text{ min}^{-1}$ .

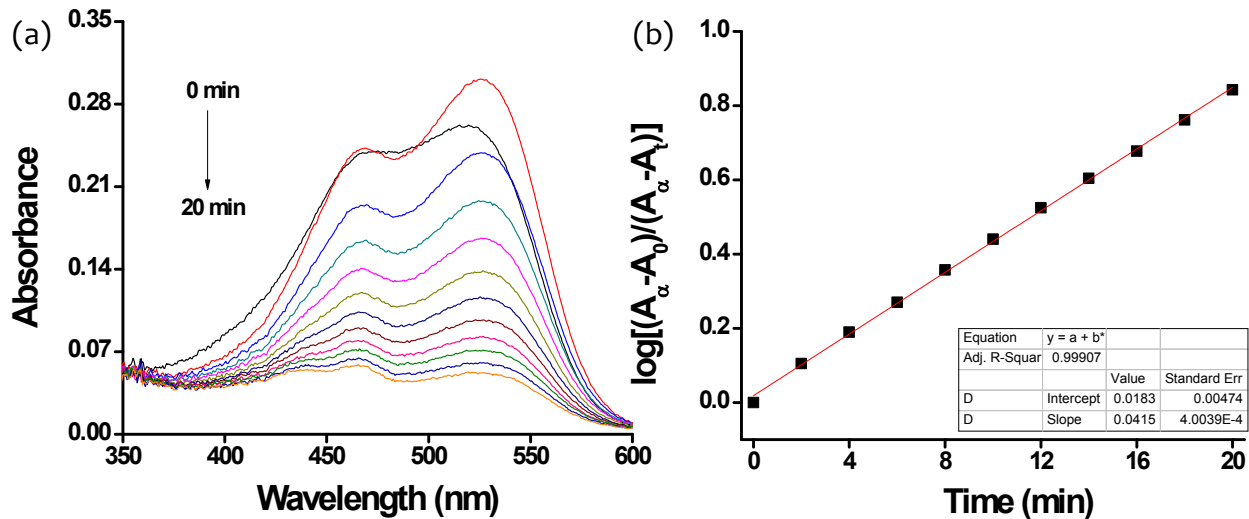


**Figure S6.** (a) Changes in UV-visible spectra of **1** (20  $\mu\text{M}$ ) with time upon addition of 0.25 mM of DCNP in water (pH 8.0) at 45  $^{\circ}\text{C}$ . (b) Plot of  $\text{Abs}_{525 \text{ nm}}$  against time shows 1st Order reaction. Rate constant:  $(9.56 \pm 0.04) \times 10^{-2} \text{ min}^{-1}$ .

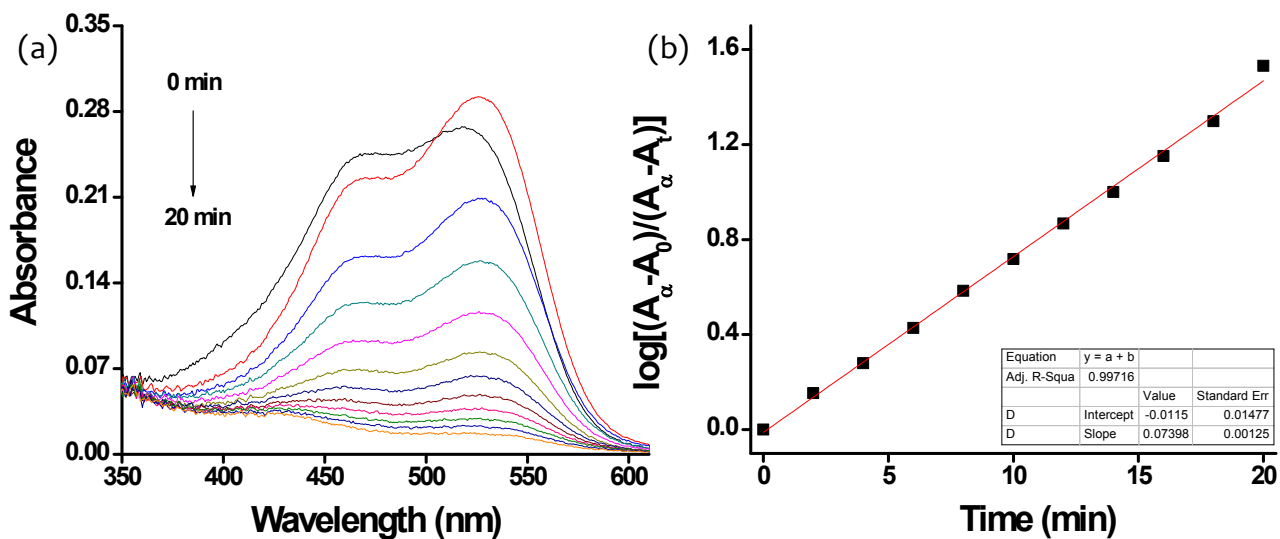


**Figure S7.** (a) Changes in UV-visible spectra of **1** (20  $\mu\text{M}$ ) with time upon addition of 0.25 mM of DCNP in water (pH 8.0) at 55  $^{\circ}\text{C}$ . (b) Plot of  $\text{Abs}_{525 \text{ nm}}$  against time shows 1st Order reaction. Rate constant:  $(17.03 \pm 0.12) \times 10^{-2} \text{ min}^{-1}$ .

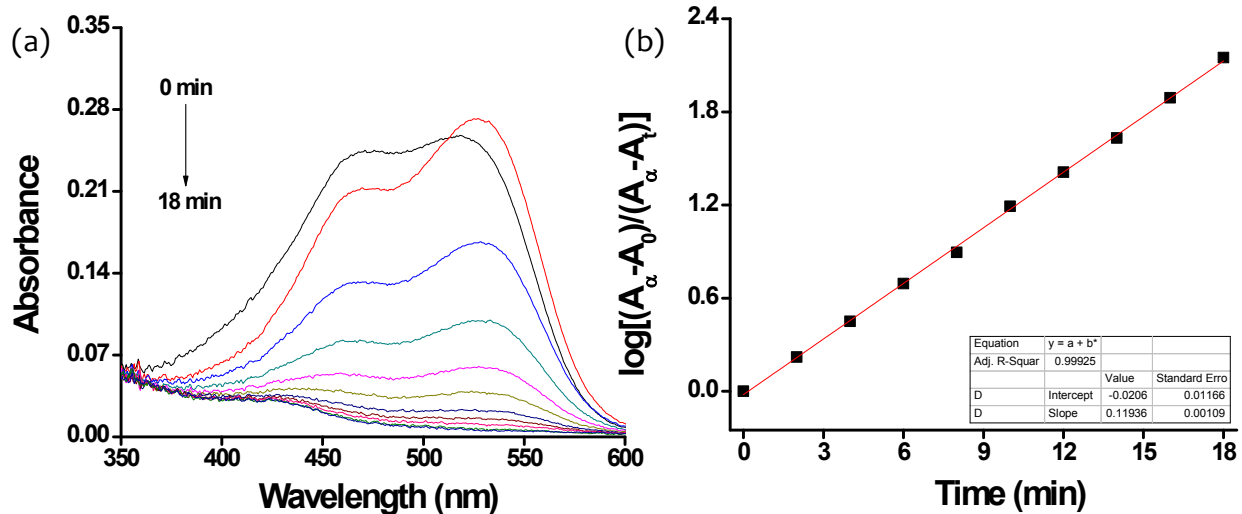


**Figure S8.** (a) Changes in UV-visible spectra of **1** (20  $\mu\text{M}$ ) with time upon addition of 0.25 mM of DCNP in water (pH 8.0) at 65  $^{\circ}\text{C}$ . (b) Plot of  $\text{Abs}_{525 \text{ nm}}$  against time shows 1st Order reaction. Rate constant:  $(27.49 \pm 0.1) \times 10^{-2} \text{ min}^{-1}$ .

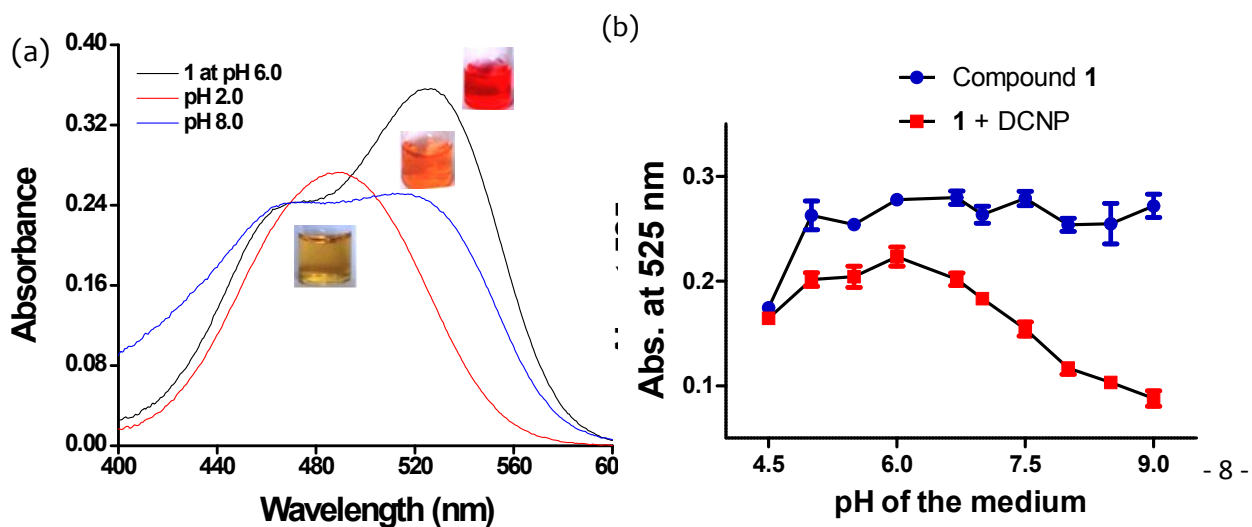




**Figure S9.** (a) Absorption spectra of **1** (20  $\mu\text{M}$ ) at different pH in water. (b) Effect of pH on interaction of **1** with DCNP (0.25 mM) at pH 8.0 in water.

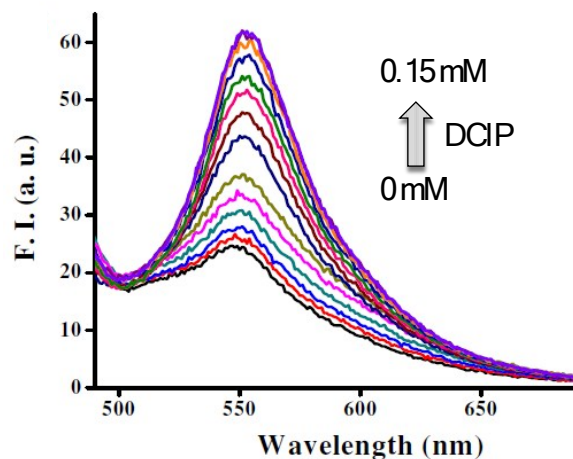


**Figure S10.** Fluorescence titration of **1** (20  $\mu\text{M}$ ,  $\lambda_{\text{ex}} = 465 \text{ nm}$ ) with DCIP (0 – 0.15 mM) in water (pH 8.0).

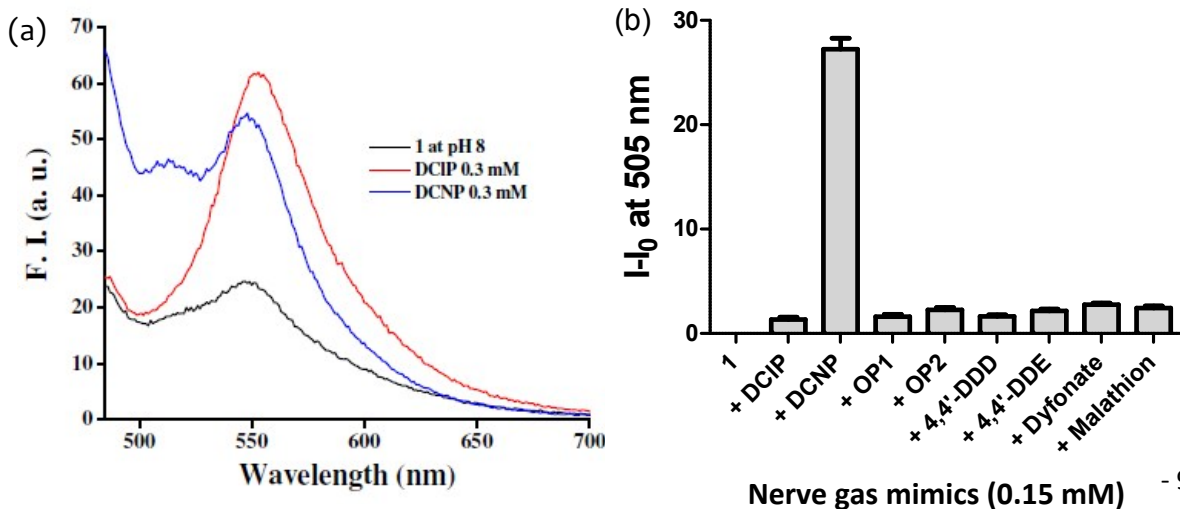


**Figure S11.** (a) Compare the effect of DCNP and DCIP on the emission spectra of **1** (20  $\mu\text{M}$ ,  $\lambda_{\text{ex}} = 465$  nm) at pH 8.0 in water. (b) Change in fluorescence intensity of **1** (20  $\mu\text{M}$ ,  $\lambda_{\text{ex}} = 465$  nm) at 505 nm upon addition of different warfare chemical agents (0.15 mM) at pH 8.0 in water.

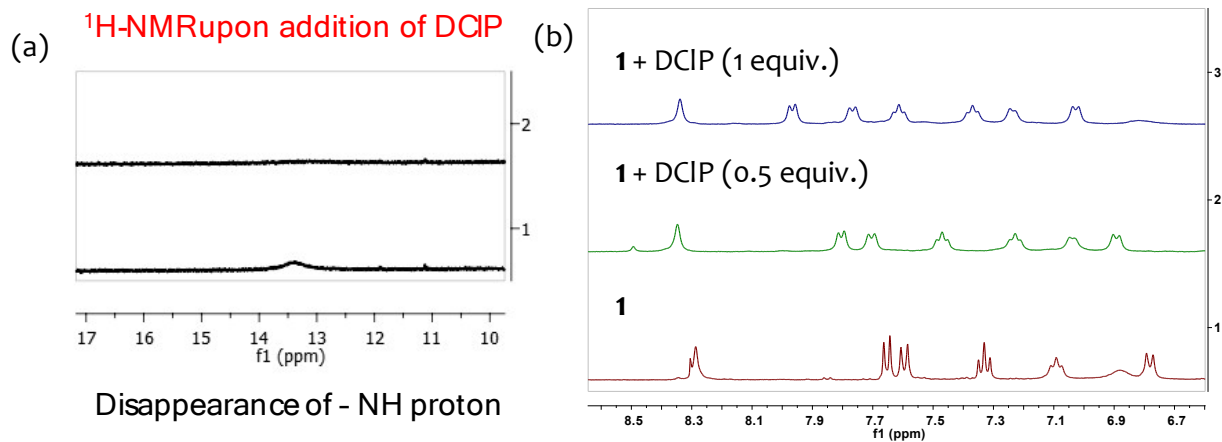


**Figure S12.** (a) DCIP induced broadening of indolyl -NH peak of **1** (2 mM) in DMSO-D<sub>2</sub>O (1:1) mixture medium. (b) Partial <sup>1</sup>H-NMR titration of **1** upon gradual addition of DCIP (1 and 2 mM) in DMSO-d<sub>6</sub>/D<sub>2</sub>O (1:1) mixture medium.

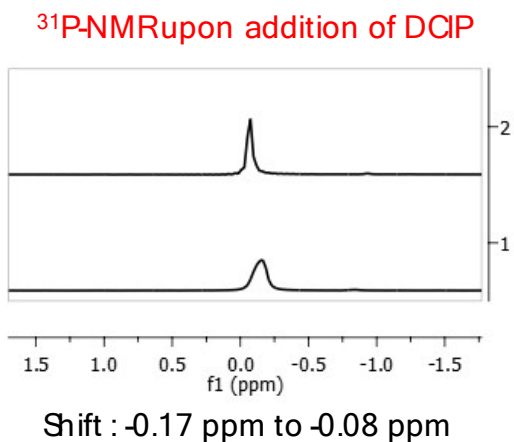


**Figure S13.** DCIP induced shift in  $^{31}\text{P}$ -NMR peak of DCIP (2 mM) upon interaction with **1** (1:1) in DMSO- $\text{D}_2\text{O}$  (1:1) mixture medium.

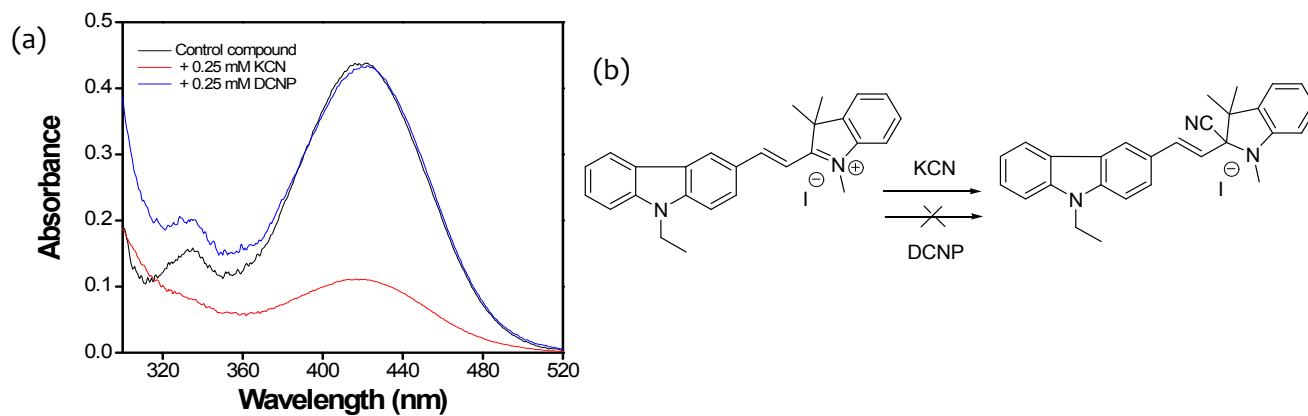


**Figure S14.** (a) Interaction of control compound **2** with KCN and DCNP (0.25 mM) at pH 8.0 in water. (b) Schematic diagram showing the cyanide adduct of compound **2**, as described in the following reference:

S. Wang, X. Fei, J. Guo, Q. Yang, Y. Li, Y. Song, A novel reaction-based colorimetric and ratiometric fluorescent sensor for cyanide anion with a large emission shift and high selectivity, *Talanta*, 2016, **148**, 229-236.

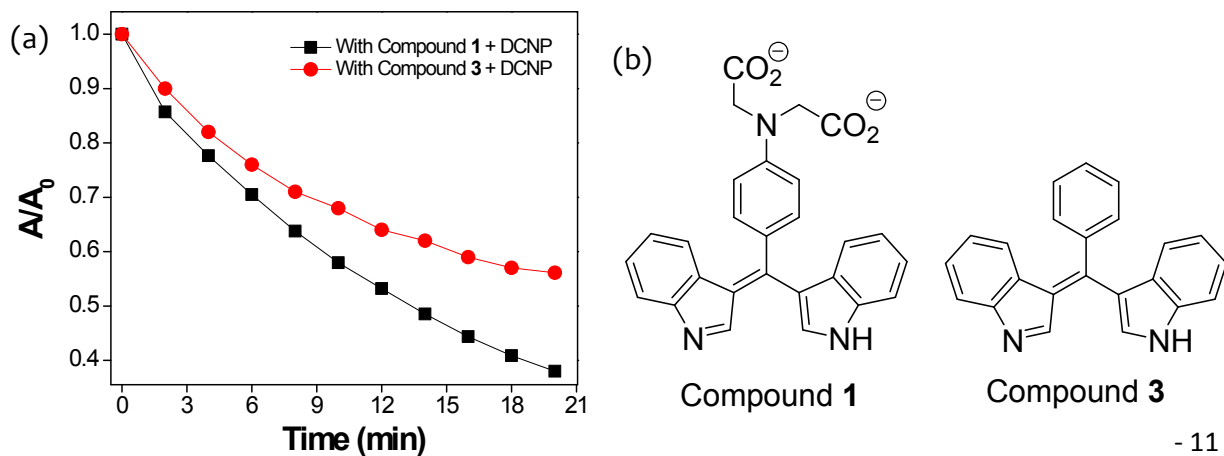


**Figure S15.** (a) Comparison of the absorption spectra of **1** (20  $\mu\text{M}$ ) in presence of DCNP (0.25 mM) with compound **3** (without having  $-\text{CO}_2^-$  group) at pH 8.0 in water. (b) Structures of compounds **1** and **3** involved in present study.

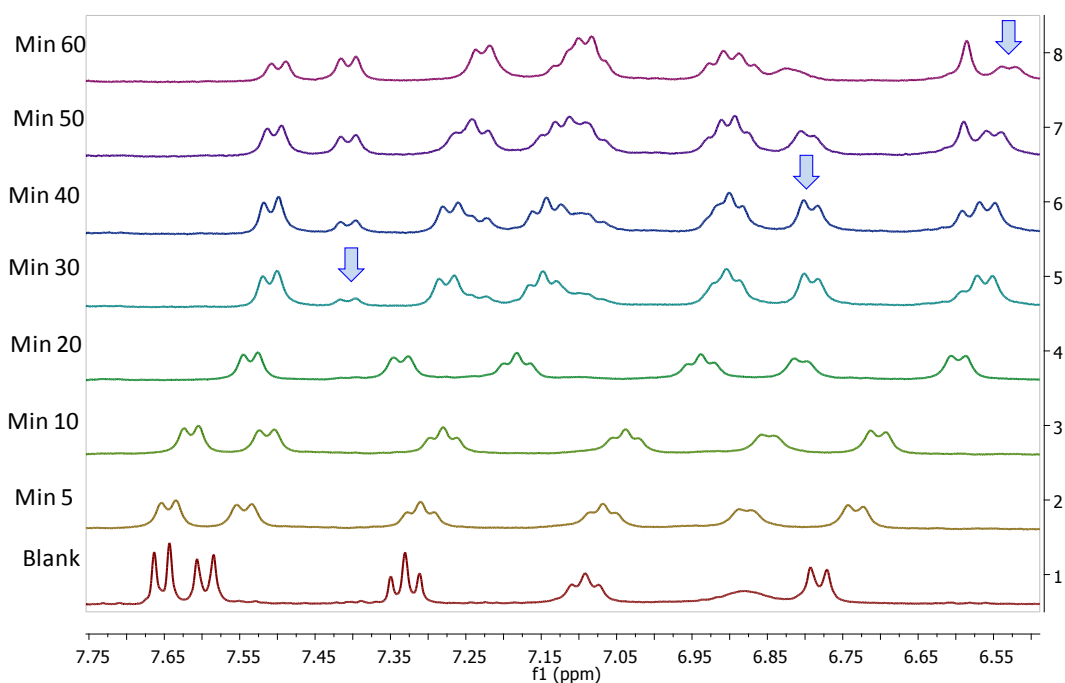


**Figure S16.** Time dependent change in  $^1\text{H}$ -NMR spectrum of **1** (2 mM) upon addition of DCNP (2 mM) in  $\text{DMSO-d}_6/\text{D}_2\text{O}$  (1:1) mixture medium.

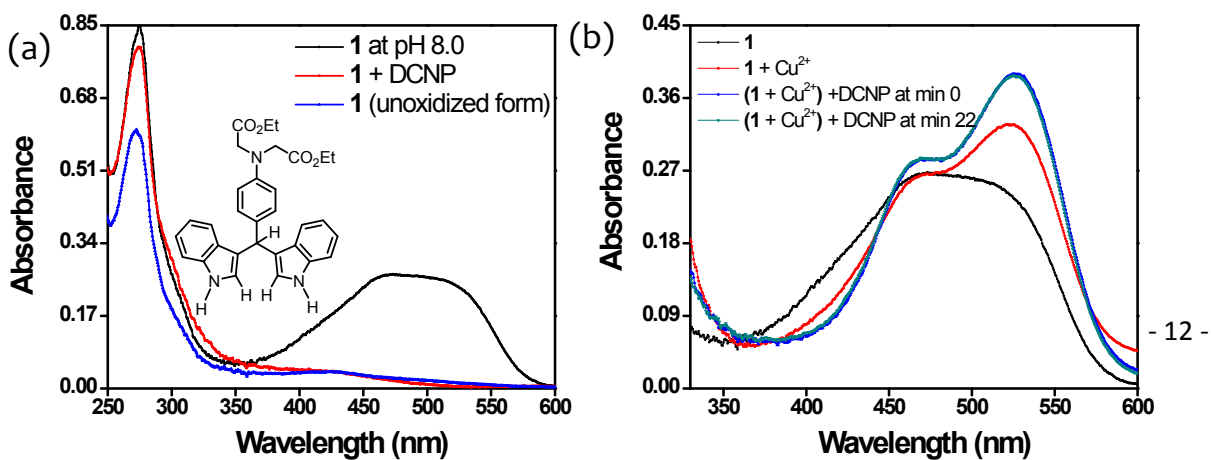


**Figure S17.** (a) Comparison of the absorption spectra of **1** (20  $\mu\text{M}$ ) in presence of DCNP (0.25 mM) with the unoxidized precursor of **1** at pH 8.0 in water. (b) Comparison of the extent of interaction of **1** (20  $\mu\text{M}$ ) with DCNP (0.25 mM) in presence of  $\text{Cu}^{2+}$  at pH 8.0 in water.

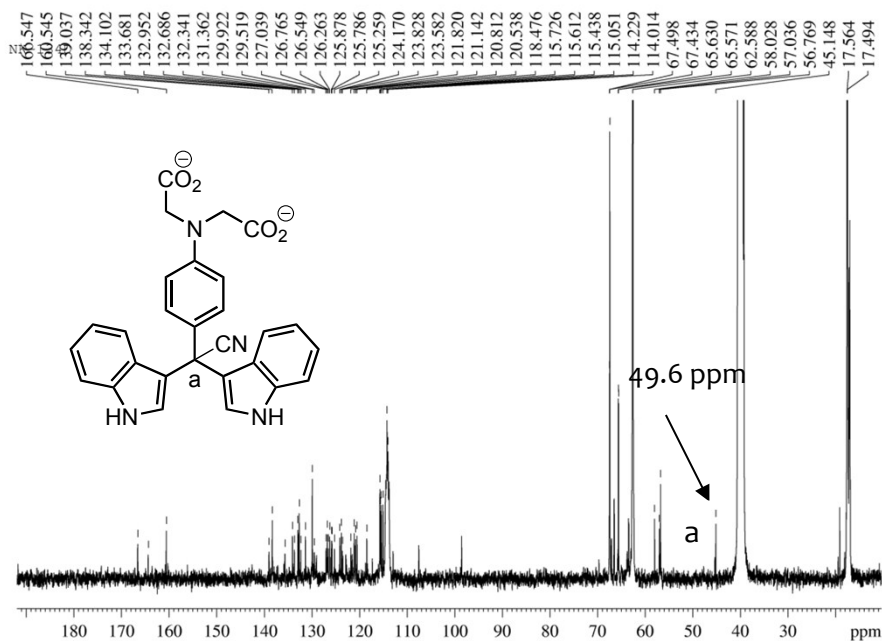


**Figure S18.**  $^{13}\text{C}$ -NMR spectra of **1** (2 mM) in presence of DCNP in DMSO- $\text{D}_2\text{O}$  (1:1) mixture medium (Inset shows the structure of cyanide adduct formed during reaction of **1** with DCNP).

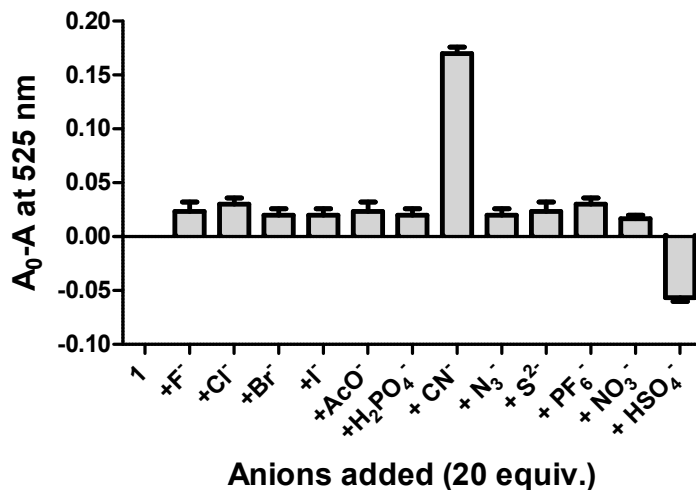


**Figure S19.** Change in absorbance of **1** (20  $\mu$ M) at 524 nm upon addition of different anions (0.2 mM) pH 8.0 in water.

### Interaction of compound **1** with DCNP in presence of KCN

At pH 8.0, the addition of KCN in the aqueous solution of **1**, showed a time dependent (~20 min) change in color from orange to colorless. This was due to the cyanide mediated Michael addition reaction to the electron deficient C=C bond of the conjugated bis-indolyl system (Figure S19). However, no immediate color change from orange to red was observed in this case. On the contrary, the addition of DCNP in presence of KCN (in 1:1 ratio) also showed an initial color change of **1** from orange to red due to indole group assisted hydrolysis of phosphoester analyte. Then a time dependent fading of color could be noticed. As the externally added cyanide ion could only increase the effective concentration of the nucleophile in the reaction medium, rates of the Michael addition reactions with DCNP were found to be almost similar both in the presence and absence of KCN.

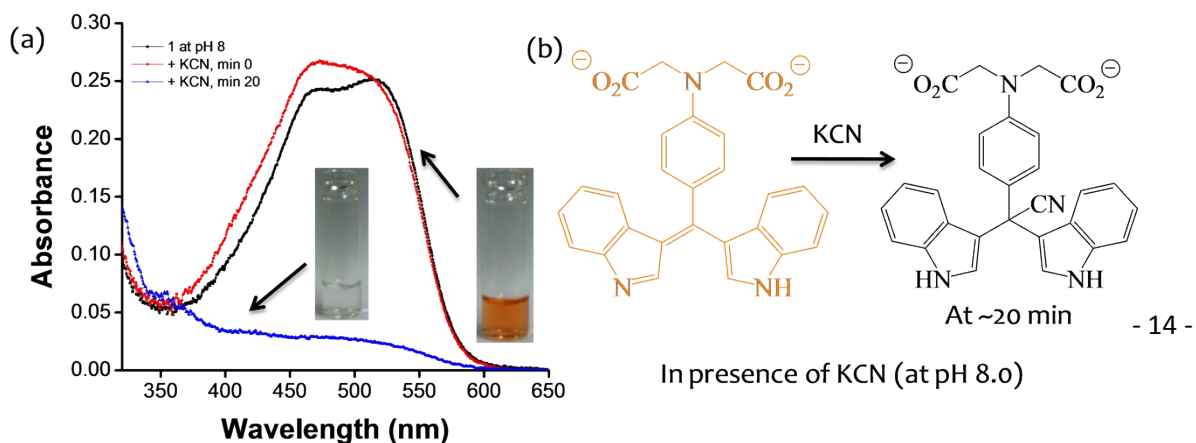


**Figure S20.** (a) UV-visible spectra of **1** (10  $\mu\text{M}$ ) in presence of KCN (0.25 mM) at pH 8.0 in water. [Inset showed color change of the aqueous solution **1** (10  $\mu\text{M}$ ) upon addition of KCN after 20 min of incubation time]. (b) Schematic diagram showing the time dependent interaction of **1** with KCN at pH 8.0 in water.

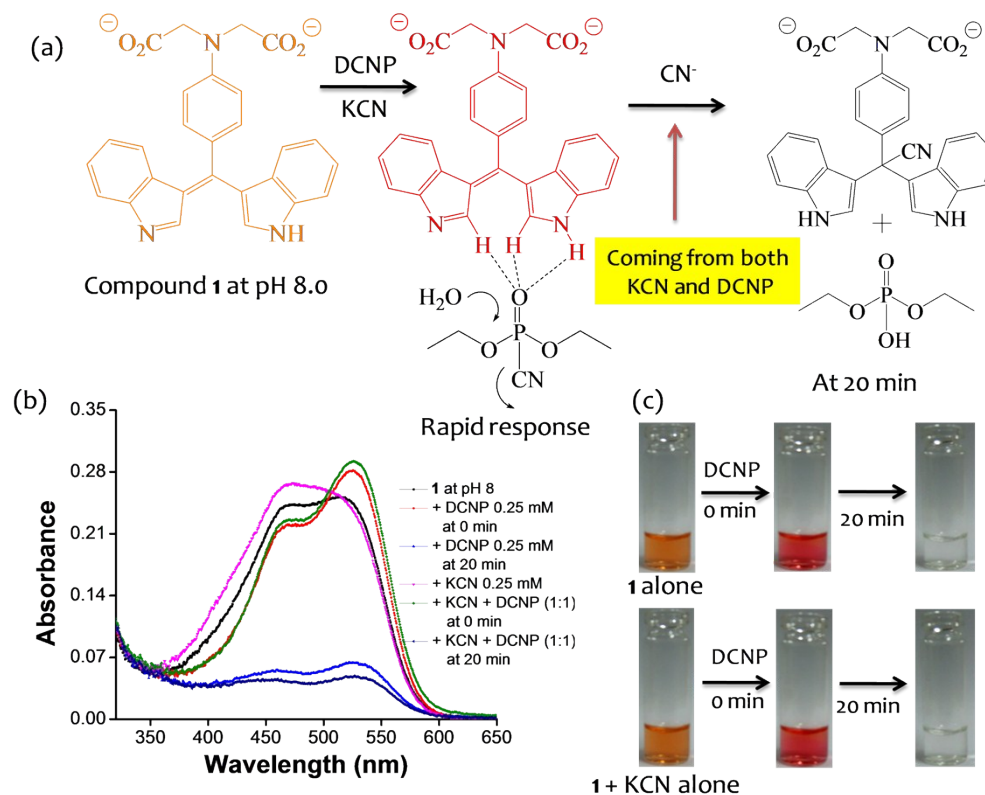


**Figure S21.** (a) Schematic diagram showing the time dependent interaction of **1** with DCNP (in presence of KCN) at pH 8.0 in water. (b) UV-visible spectra of **1** (10  $\mu\text{M}$ ) in presence of DCNP (0.25 mM) at pH 8.0 in water (both in presence and absence of KCN). (c) Color change of the aqueous solution **1** (10  $\mu\text{M}$ ) upon addition of DCNP both in presence and absence of KCN at pH 8.0 in water.

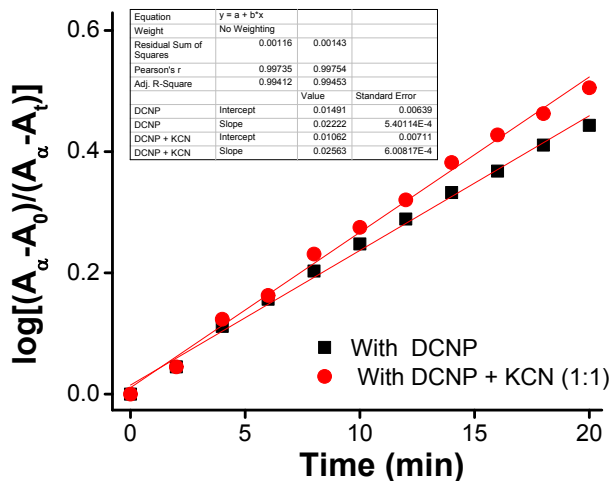


**Figure S22.** Plot of  $Ab_{S_{25\text{ nm}}}$  against time shows 1st Order reaction. Rate constant:  $(5.06 \pm 0.05) \times 10^{-2} \text{ min}^{-1}$  without DCNP and  $(5.89 \pm 0.04) \times 10^{-2} \text{ min}^{-1}$  with mixture of DCNP + KCN (1:1).

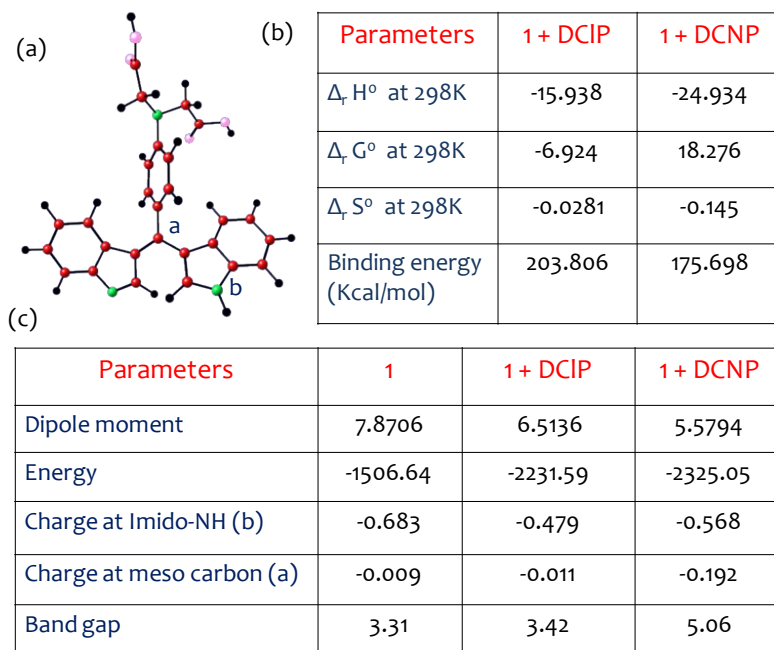


**Figure S23.** (a) Energy minimized structure of **1** using B3LYP/6-31 G\* level of theory. (b) Estimation of different thermodynamic parameters corresponding to the interaction of **1** with DCNP and DCIP in water (PCM model). (c) Determination of structural parameters associated with energy minimized adducts of **1** with DCNP and DCIP in water (PCM model).

Upon complexation with DCIP, the bridging carbon center (meso) of **1** remained in  $sp^2$  hybridized state; hence the planar conformation was conserved with  $120^\circ$  bond angle. On the contrary, in the case of DCNP, the nucleophilic attack of cyanide converted the hybridization of this center from  $sp^2$  to  $sp^3$  with a bond angle of  $108^\circ$  (nonplanar tetrahedral geometry). This change in hybridization can affect the optical bandgaps of the corresponding adducts in solution.



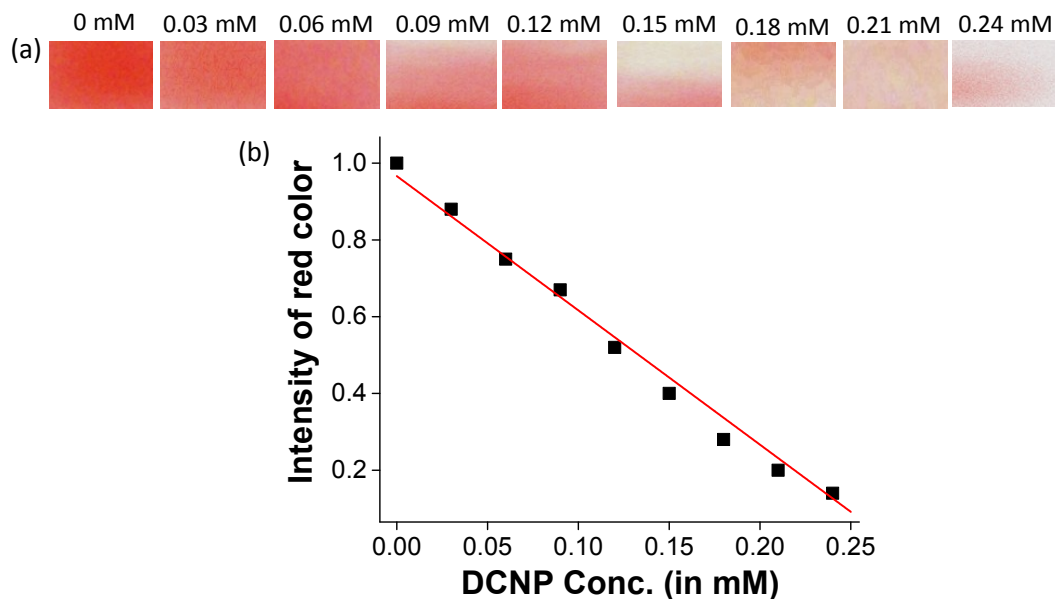


**Figure S24.** (a) Discoloration of color strips in presence of DCNP at pH 8.0 in water, the concentrations have been mentioned on the top of the strips (incubation time in each case was 30 min). (b) Quantification of color change using ImageJ software.

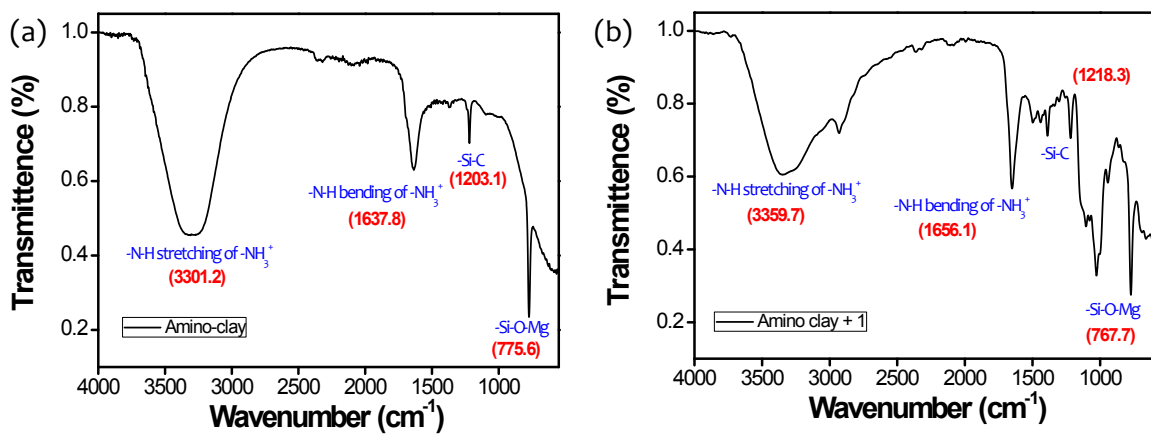


**Figure S25.** FT-IR spectra of (a) compound 1 and (b) 1 + amino clay conjugate in water.

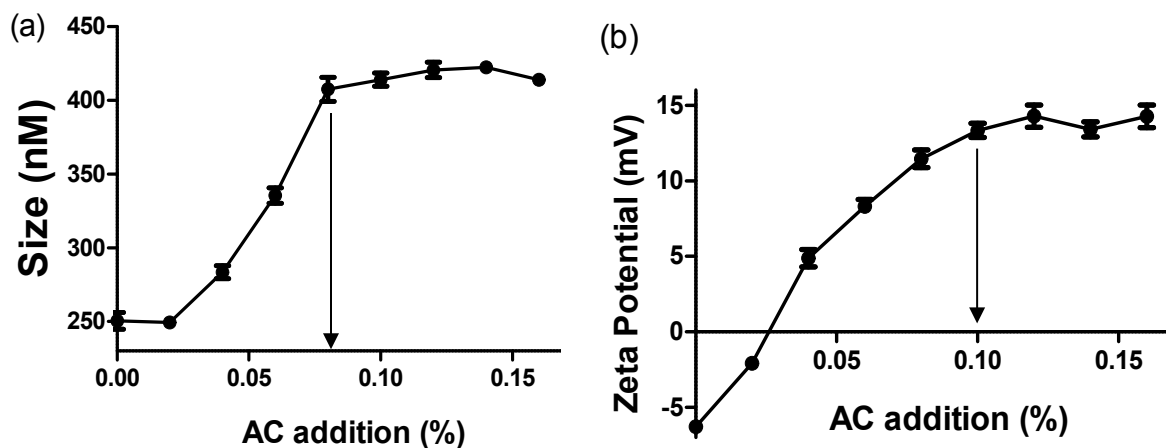


**Figure S26.** (a) Variations in size (hydrodynamic diameter) of **1** upon gradual addition of amino clay in water. (b) Variations in zeta potential of **1** upon gradual addition of amino clay in water.

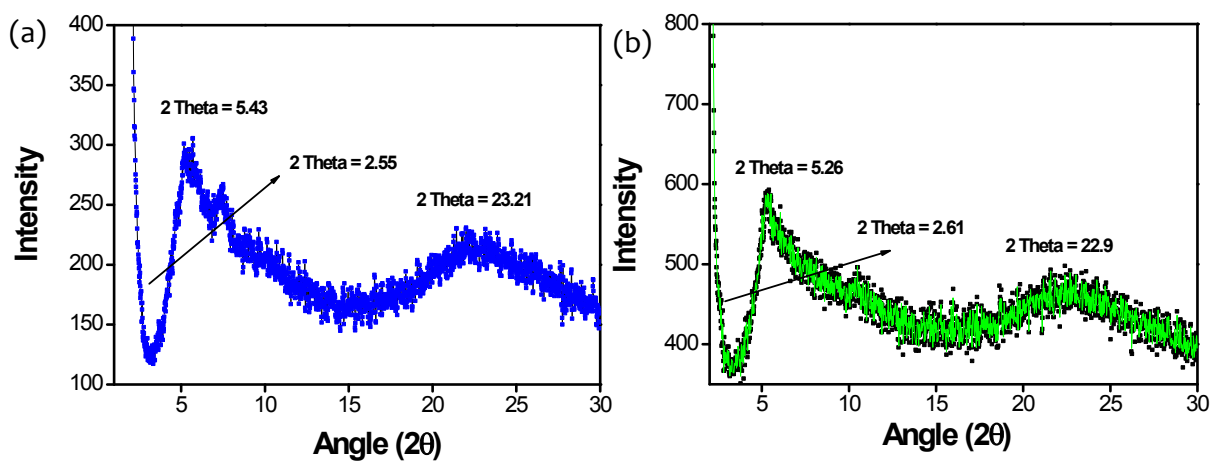


**Figure S27.** PXR D patterns of compound (a) **1** and (b) **1** + amino clay conjugate. [Low angle interlayer  $d_{001}$  reflection at 1.6 nm broad peaks at 3.96 nm ( $d_{130,200}$ ) and 0.155 nm ( $d_{060,330}$ ), consistent with a partially disordered layered structure typically observed in this class of synthetic organoclays.  $2\theta = 5.43$ ;  $d = 1.62$  nm,  $2\theta = 2.55$ ;  $d = 3.46$  nm,  $2\theta = 23.2$ ,  $d = 0.38$  nm].

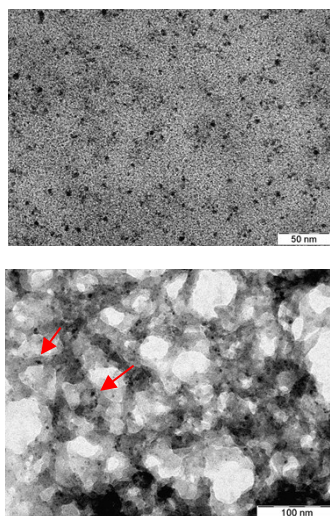


**Figure S28.** TEM images of **1** (20  $\mu\text{M}$ , top image) and **1** + AC ([**1**] = 20  $\mu\text{M}$  & [AC] = 0.1%, bottom image) in water.

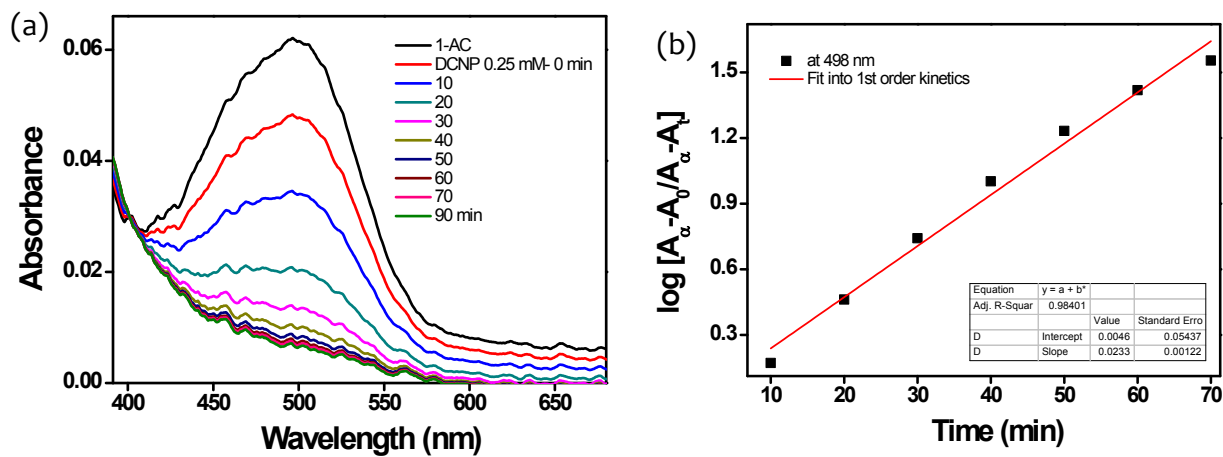


**Figure S29.** (a) Time dependent change in UV-visible spectra of **1** + AC conjugate ( $[1] = 20 \mu\text{M}$ , AC = 0.1%) upon addition of 0.25 mM DCNP in water. (b) Determination of rate of interaction from 1<sup>st</sup> order rate kinetic equation. Rate constant =  $(5.37 \pm 0.12) \times 10^{-2} \text{ min}^{-1}$ .

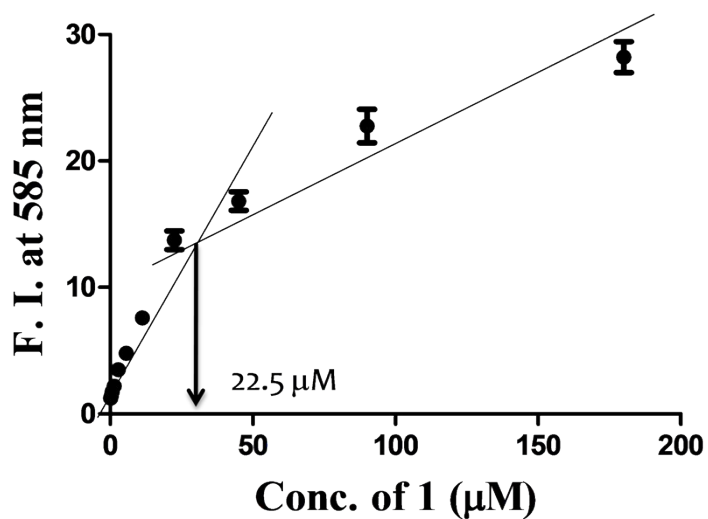


**Figure S30.** Change in emission intensity of **1** ( $\lambda_{\text{ex}} = 465 \text{ nm}$ , monitored at 585 nm) upon variation of concentration in water.

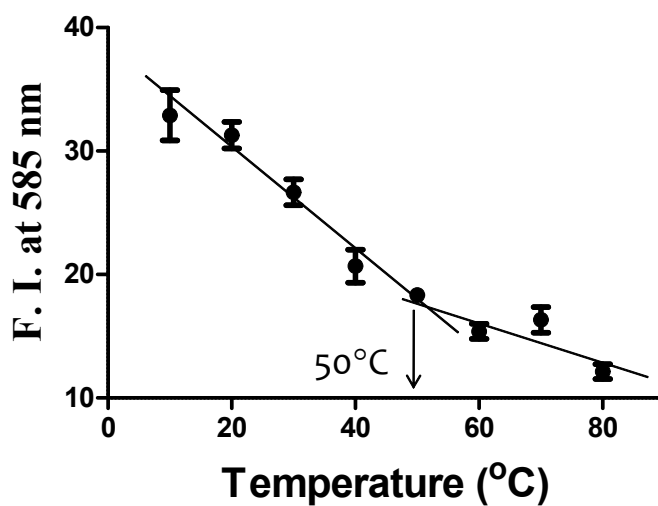


**Figure S31.** Change in emission intensity of **1** (150  $\mu\text{M}$ ,  $\lambda_{\text{ex}} = 465 \text{ nm}$ ) at 585 nm upon variation of temperature in water.

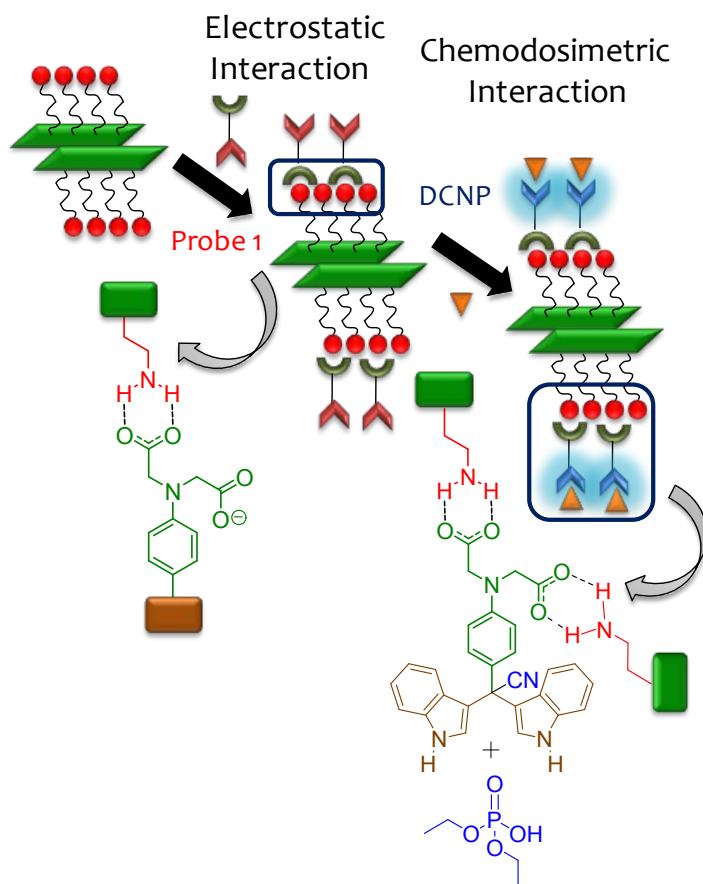


**Figure S32.** Schematic diagram showing the interaction of DCNP with **1**+AC conjugate in water.

#### Advantages of incorporating amino clay in the present case:

1. Compound **1**, due to its planer, amphipathic structure, showed prominent tendency to form self-aggregate in water, which made some of the binding sites unavailable for interaction with DCNP. The addition of amino clay (AC) could destroy these preformed random agglomerates and allowed the probe molecules to be systematically reorganized onto its cationic surface. This accordingly exposed number of binding sites towards DCNP and enhanced the sensitivity to a great extent.
2. The presence of aminopropyl units onto the surface of AC could also catalyze the hydrolysis of the nerve gas mimicking agents. This would increase the effective concentration of the nucleophile (free cyanide ion) in the reaction medium and shift the equilibrium more towards the product side. [Ref: Barba-

Bon, A.; Martinez-Manez, R.; Sancenon, F.; Costero, A. M.; Gil, S.; Perez-Pla, F.; Llopis, E. *J. Hazard. Mater.*, **2015**, 298, 73–82.]

3. As the interaction with cyanide ion could cut-off the overall conjugation, it was expected to receive a ‘turn on’ emission response in presence of DCNP due to restriction in the charge transfer process. However, the enhancement was very less in water due to high conformational flexibility of the resultant tetrahedral adduct (increase in the number of non-radiative decay). On the other hand, low conformational flexibility of the 3,3 -Diindolylmethane moiety in the **1** + AC conjugate could be presumed as the reason for the drastic emission enhancement. [Ref: Jain, A.; Achari, A.; Mothi, N.; Eswaramoorthy, M.; George, S. J. Shining light on clay–chromophore hybrids: layered templates for accelerated ring closure photo-oxidation. *Chem. Sci.*, **2015**, 6, 6334-6340.]

4. The relatively high hydrophobic environment around the probe in **1** + AC conjugate also diminished the chances of solvent mediated emission quenching.

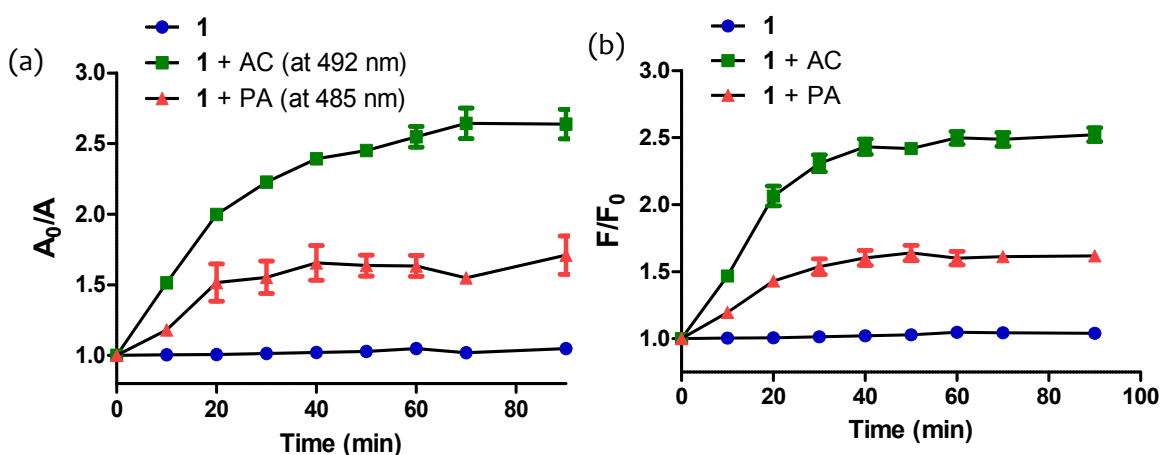
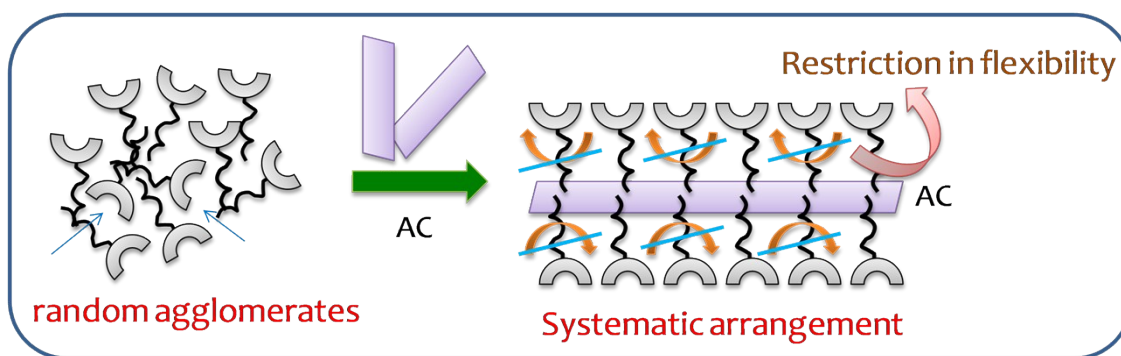


**Figure S33.** Compare the extent of interaction of **1**, **1** + amino clay (AC) and **1** + propyl amine (PA) conjugate ( $[1] = 20 \mu\text{M}$  in every case) with DCNP in water (a) through UV-visible studies and (b) Fluorescence studies.